CHAPTER III

OZONE DISSOCIATION: PHOTO-DISSOCIATION AND SURFACE INDUCED DISSOCIATION

3.1 INTRODUCTION

Ozone dissociation is an integral part of ozone formation during UV photolysis. Therefore, in addressing the issue of isotopic enrichment of ozone (as described in Chapter II; Bhattacharya et al., 2002), it is important to characterize its different dissociation channels. The relevant dissociation pathways are: i) photo-dissociation, ii) thermal dissociation, iii) dissociation by chemical reactions and iv) dissociation through surface interaction. Among these four, thermal dissociation was studied in detail by Wen and Thiemens (1991) and Kim and Yang (1997). Their studies show some intriguing aspects during ozone dissociation in gas phase. Below 90^{o}C, thermally dissociated ozone yields isotopically light oxygen and the left-over ozone is enriched in a mass-dependent fashion. Above 90^{o}C, the isotopic behavior flips and the product oxygen becomes heavier in a mass independent fashion. The isotopic characteristic of thermal dissociation products is still an open question from theoretical point of view.

Dissociation of ozone by chemical reactions was studied recently (Chakraborty and Thiemens, Personal Communication). The left-over ozone shows a normal mass-dependent enrichment, as seen in most of the chemical reactions.

Among the other two dissociation pathways, two earlier studies dealt with photo-dissociation of ozone by UV and visible light (Bhattacharya and Thiemens, 1988; Wen and Thiemens, 1991), which showed slight deviation from mass dependence in the case of UV dissociation. The present chapter deals with these two pathways of ozone dissociation. In Part A, photo-dissociation will be discussed and in Part B, surface induced ozone dissociation will be covered.

3.2 PART A: PHOTO-DISSOCIATION OF OZONE

3.2.1 Motivation

The previous photo-dissociation experiments by Bhattacharya and Thiemens (1988) and Wen and Thiemens (1991) show that photo-dissociation of ozone produces isotopically light oxygen with respect to the initial ozone. Due to limited number of data points in the UV dissociation experiment of Bhattacharya and Thiemens (1988), the slope ($\Delta\delta^{17}O/\Delta\delta^{18}O$) could not be firmly established to probe the isotopic behavior of ozone during UV dissociation. The results of photo-dissociation experiments using UV and visible light by Wen and Thiemens (1991) are quite interesting. They suggest that UV dissociation results in oxygen with mass independent character, whereas, dissociation in

visible wavelengths is strictly a mass dependent process. But detailed characterization of the mass independent fractionation in UV dissociation is still required to better comprehend the causative factors.

The motive behind the present experiments is two-fold: first, a better characterization of the fractionation in photo-dissociation of ozone in UV (Hartley band) and visible wavelengths (Chappuis band) and second, search for the cause behind the anomalous fractionation in UV photo-dissociation process from an experimental perspective.

3.2.2 Experimental Procedure

Photolysis of ozone was done using UV (184.9 and 253.6 nm from Hg resonance lamp) and visible (520 and 630 nm) wavelengths for various periods (from 2 to 12 minutes for UV light and 60 to 1500 minutes for visible light). In all the experiments, ozone was first produced in a 5-liter spherical chamber fitted with a MgF_2 window (experimental set-up same as described in § 2.2.1) by irradiating ultra-pure oxygen with UV generated by a Hg resonance lamp (184.9 and 253.6 nm) driven by a micro-wave generator. After irradiation, the product ozone was frozen by LN_2 in a cold finger attached with the flask and the oxygen pumped away till 2 mtorr pressure (vapor pressure of ozone at LN_2) was obtained.

Three sets of experiment were carried out. In set 1, ozone was produced at 500 torr oxygen pressure for 200 to 400 minutes. Each time, the isotopic composition of the product ozone was determined by taking an aliquot by equilibrating the ozone with a separate 1-liter chamber connected to the 5-liter chamber through stopcocks. Since the oxygen pressure was always 500 torr the isotopic composition of the ozone was reasonably constant within $\delta^{17}O = 93.7 \pm 1.5$ and $\delta^{18}O = 97.0 \pm 1.6$ ‰ (with respect to a laboratory working gas). The amount of ozone produced varied from 434 to 1025 μmole (oxygen equivalent) depending on the time of UV irradiation. The isotopically characterized product ozone was considered as the initial ozone and irradiated by UV photons from the Hg resonance lamp (184.9 and 253.7 nm) for 2 to 12 minutes to dissociate its different fraction.

In set 2, ozone was produced by irradiating ultra-pure oxygen at 500 torr pressure for ~ 120 minutes. As before, each time the isotopic composition of the product ozone was determined by taking an aliquot from the 5-liter chamber and the values were 95.2 ±

1 and 95.9 ± 0.2 ‰ for $\delta^{17}O$ and $\delta^{18}O$ respectively. Next, ultra pure nitrogen was added in steps from 10 to 80 torr to the ozone within the 5-liter chamber in different experiments and irradiated by UV photons from a Hg resonance lamp (184.9 and 253.6 nm) for 3 to 4 minutes.

In set 3, ozone was produced at 240 torr oxygen pressure for 60 minutes (except for one case where the irradiation time was increased to 80 minutes). The amount of product ozone and its isotopic composition was determined once during this set of experiment. The irradiation protocol (60 minutes with input power 70 watts and reflected power 10 watts) was strictly maintained to ensure retrieval of the same amount and isotopic composition of ozone (~ 55 ± 7 μmole with $\delta^{17}O$ = 104 ± 3 ‰ and $\delta^{18}O$ = 106 ± 2 ‰). The product ozone was irradiated by halogen filled tungsten lamp fitted with two different interference filters providing photons at wavelength range 520 ± 2 nm and 630 ± 4 nm in two different sub-sets of experiment; irradiation was done for 60 to 1500 minutes to dissociate different fractions of ozone.

In all the three sets of experiment, after the irradiation, the left-over ozone was frozen by LN_2 in the bottom trap of the chamber and the product oxygen (formed by ozone dissociation) was collected in a sample bottle (1 cc) containing molecular sieve with LN_2. After the collection of product oxygen, the left-over ozone was released and collected in another sample bottle (1 cc) containing molecular sieve in a similar way. Heating and refreezing for 3 to 4 times converted the ozone to oxygen.

Isotopic ratios and the yield of ozone (as oxygen) were measured using a GEO 20-20 (Europa Scientific) mass-spectrometer following the procedure described in § 2.2.2. Considering transfers of gases, aliquot separation and several freezing and thawing processes, the error in determining the isotopic ratio is slightly higher than the analytical error due to mass spectrometer alone. We estimate an overall uncertainty of 0.1 ‰ for $\delta^{18}O$ and 0.2 ‰ for $\delta^{17}O$ for the final data based on few repeat measurements.

3.2.3 Results

The results of the photo-dissociation experiments using UV and visible wavelengths (set 1 to 3) are given in Tables 3.1, 3.2 and 3.3 respectively and show that the left-over ozone is enriched in both ^{17}O and ^{18}O with respect to the initial ozone in all the three sets of experiments. On the other hand, the product oxygen (measured in set 1 and set 3 experiments) is depleted and the depletion increases with increasing irradiation

time, i.e. with increase of the extent of dissociation. For set 1 (UV dissociation), at 98 % dissociation level, the enrichments in ^{17}O and ^{18}O in the left-over ozone pool are about 50.1 and 79.5 ‰ respectively (Table 3.1). In contrast, for set 3 (visible light dissociation), at 81 % dissociation level, the enrichments in ^{17}O and ^{18}O are about 16.7 and 29.9 ‰ respectively (Table 3.3), which are much lower compared to the values in set 1 for equivalent dissociation level.

Figures 3.1a and 3.1b show the covariation plot between $\Delta\delta^{17}O$ and $\Delta\delta^{18}O$ for product oxygen and left-over ozone for set 1 and set 3 experiments. The slopes of the covariation plots for these two sets are different. The visible light dissociation of set 2 (Figure 3.1b) depicts a strictly mass dependent slope (0.54 ± 0.01), whereas the UV dissociation of set 1 (Figure 3.1a) shows an increased value of the slope (0.63 ± 0.01).

In order to determine the fractionation factor α for the dissociation processes described in sets 1 and 3, we assume that the progressive variation in fractionation follows a Rayleigh model of the form $R = R_o f^{(\alpha-1)}$ (similar to § 2.3). Here R_o and R are the initial and final $^{18}O/^{16}O$ ratios (of O_3) respectively and f is the fraction of O_3 left. Writing in δ notation and taking natural logarithm:

$$\ln(1 + 0.001 \times \delta) = \ln(1 + 0.001 \times \delta_o) + (\alpha - 1) \ln(f) \qquad (3.1)$$

Where δ_o and δ are the $\delta^{18}O$ of initial and final ozone respectively. Figures 3.2a and 3.2b show the plot of $\Delta\ln(1 + 0.001 \times \delta)$ $(= \ln(1 + 0.001 \times (\delta^{18}O)) - \ln(1 + 0.001 \times (\delta^{18}O)_o))$ against ln(f) for sets 1 and 3 respectively. A best-fit line through the points yields values for the instantaneous fractionation factor α, 1.0176 and 1.0151 for set 1 and 3 respectively. These values imply that for UV dissociation the ^{18}O containing isotopomers of ozone dissociate with a rate 1.76 % lower compared to only ^{16}O containing isotopomers. And for the visible light dissociation the same rate is lower by 1.51 %.

Table 3.1. *Oxygen isotopic fractionation in products of UV dissociation of ozone using Hg Lamp*

Amount of initial ozone (µmole)	Initial ozone		Amount of product oxygen (µmole)	Product oxygen				Amount of Left-over ozone (µmole)	Left-over ozone				
	$\delta^{17}O$ (‰)	$\delta^{18}O$ (‰)		$\delta^{17}O$ (‰)	$\delta^{18}O$ (‰)	$\Delta\delta^{17}O$ (‰)	$\Delta\delta^{18}O$ (‰)		$\delta^{17}O$ (‰)	$\delta^{18}O$ (‰)	$\Delta\delta^{17}O$ (‰)	$\Delta\delta^{18}O$ (‰)	Slope* ($\Delta\delta^{17}O/\Delta\delta^{18}O$)
720	91.1	97.5	198	80.7	80.6	-10.4	-16.9	522	95.8	105.0	4.7	7.5	0.63
434	93.0	95.2	173	82.2	79.8	-10.8	-15.4	261	98.5	104.4	5.5	9.2	0.60
756	94.7	98.8	456	86.6	86.2	-8.1	-12.6	300	103.9	113.6	9.2	14.8	0.62
482	92.8	94.7	329	87.0	85.5	-5.8	-9.2	153	105.6	114.6	12.8	19.9	0.64
830	92.7	96.4	644	87.8	88.9	-4.9	-7.5	186	109.8	122.7	17.1	26.3	0.65
750	96.3	99.7	594	91.5	92.1	-4.8	-7.6	156	114.9	128.8	18.6	29.1	0.64
670	93.8	96.4	642	92.2	93.7	-1.6	-2.7	28	131.4	156.1	37.6	59.7	0.63
1025	95.0	97.3	1005	94.0	95.7	-1.0	-1.6	20	145.1	176.8	50.1	79.5	0.63

* After propagation of errors, the uncertainty in individual slope value is about 10 %.

***Table 3.2**. Oxygen isotopic fractionation in products of UV dissociation of ozone using Hg Lamp in presence of nitrogen at different pressures*

Amount of initial ozone (μmole)	Initial ozone		Nitrogen pressure (torr)	Amount of Left-over ozone (μmole)	Left-over ozone				
	$\delta^{17}O$ (‰)	$\delta^{18}O$ (‰)			$\delta^{17}O$ (‰)	$\delta^{18}O$ (‰)	$\Delta\delta^{17}O$ (‰)	$\Delta\delta^{18}O$ (‰)	Slope* ($\Delta\delta^{17}O/\Delta\delta^{18}O$)
370	93.8	96.4	NIL	96	108.7	120.0	14.9	23.6	0.63
345	95.2	95.2	20	107	101.1	105.3	5.9	9.5	0.62
385	93.4	93.4	26	101	98.9	103.8	5.5	7.7	0.71
173	96.0	96.0	30	73	101.4	103.1	5.4	7.1	0.76
380	94.8	95.9	36	78	102.9	105.5	8.1	9.6	0.84
302	95.8	95.8	40	55	108.7	108.8	12.9	13.0	0.99
360	96.0	96.0	40	122	105.0	105.0	9.0	9.0	1.00
285	95.1	95.6	60	77	105.3	105.9	10.2	10.3	0.99
325	95.1	96.2	80	195	99.3	100.4	4.2	4.2	1.00

* After propagation of errors, the uncertainty in individual slope value is about 10 %.

Table 3.3. *Oxygen isotopic fractionation in products of Visible light dissociation of ozone.*

Amount of initial ozone (μmole)	Initial ozone		Amount of product oxygen (μmole)	Product oxygen				Amount of Left-over ozone (μmole)	Left-over ozone				
	$\delta^{17}O$ (‰)	$\delta^{18}O$ (‰)		$\delta^{17}O$ (‰)	$\delta^{18}O$ (‰)	$\Delta\delta^{17}O$ (‰)	$\Delta\delta^{18}O$ (‰)		$\delta^{17}O$ (‰)	$\delta^{18}O$ (‰)	$\Delta\delta^{17}O$ (‰)	$\Delta\delta^{18}O$ (‰)	Slope* ($\Delta\delta^{17}O/\Delta\delta^{18}O$)
White Light													
52.6	100.8	102.8	36.6	95.5	93.2	-5.3	-9.6	16.0	113.0	124.8	12.2	22.0	0.55
Red Light (630 ± 4 nm)													
62.2	100.3	103.0	8.6	87.2	79.3	-13.1	-23.7	53.6	102.4	106.8	2.1	3.8	0.55
52.2	102.0	104.8	11.0	90.0	83.1	-12.0	-21.7	41.2	105.2	110.6	3.2	5.8	0.55
41.7	102.6	105.2	20.2	95.2	90.7	-7.5	-14.5	21.5	109.6	118.8	7.0	13.6	0.51
67.7	110.9	107.1	54.9	107.0	100.1	-3.9	-7.0	12.8	127.6	137.0	16.7	29.9	0.56
Green Light (520 ± 2 nm)													
55.1	103.8	108.8	10.9	91.6	87.1	-12.2	-21.7	44.2	106.8	114.2	3.0	5.4	0.56
48.5	104.5	107.3	17.0	95.4	90.3	-9.1	-17.0	31.5	109.4	116.4	4.9	9.1	0.54
45.0	105.3	105.3	17.0	95.5	86.0	-9.8	-19.3	28.0	111.2	117.1	6.0	11.7	0.51
50.6	104.2	107.6	29.3	96.9	94.3	-7.3	-13.3	21.3	114.2	125.8	10.0	18.2	0.55
80.7+	106.3	104.3	62.2	102.2	96.7	-4.1	-7.6	18.5	119.9	129.8	13.6	25.5	0.53

* After propagation of errors, the uncertainty in individual slope value is about 10 %.
+ During the production of ozone, irradiation time was increased to 80 minutes

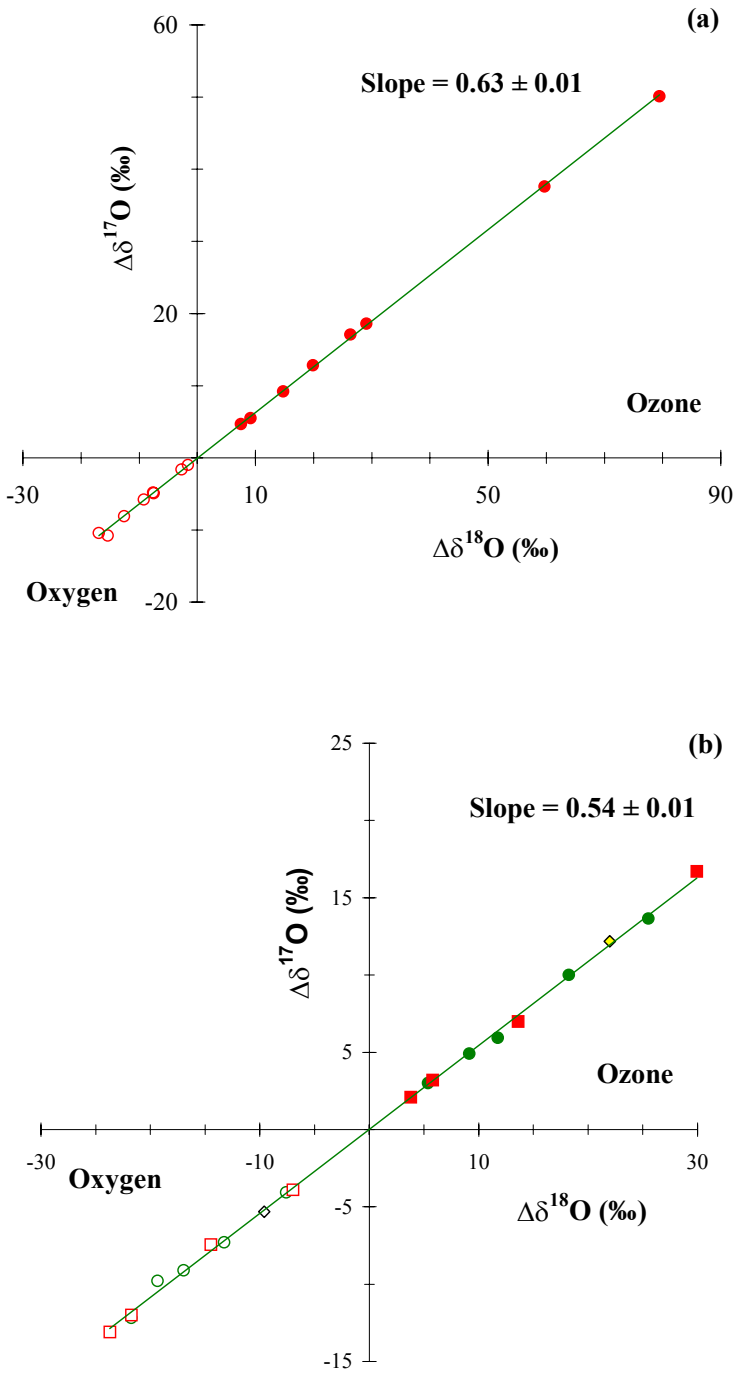

Figure 3.1. *Covariation plot between $\Delta\delta^{17}O$ and $\Delta\delta^{18}O$ for the photo-dissociation experiments. (a) For UV dissociation (using a Hg lamp) the left-over ozone (the filled circles) is enriched with respect to the initial ozone and the product oxygen (unfilled circles) is depleted. The best-fit line gives a slope of 0.63 ± 0.01 reflecting that the UV dissociation of ozone has a significant mass-independent component. (b) For the visible light dissociation at 520 (circles) and 630 (squares) nm (filled and unfilled symbols are for the left-over ozone and product oxygen respectively). The best-fit line gives a slope of 0.54 ± 0.01 indicating that the visible light dissociation of ozone is a mass-dependent process. The error of each data point is comparable to the size of the symbol.*

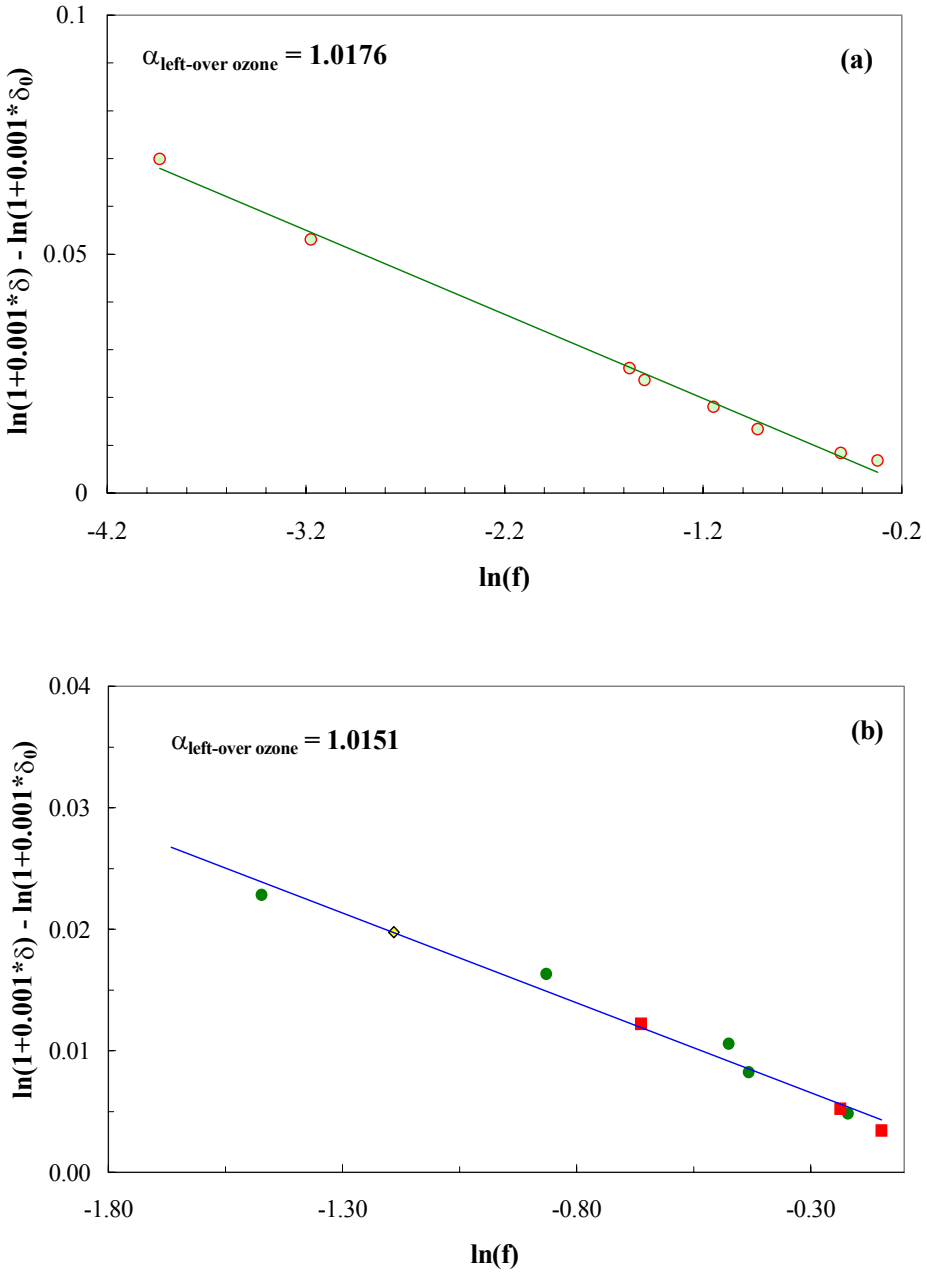

Figure 3.2. *Plot to calculate the instantaneous fractionation factor (α) for dissociation using a simple Rayleigh model: lnR= lnR$_{0}$ + (α-1) ln f. The symbols are described in the text. (a) For UV dissociation, the best-fit line yields α = 1.0176 for the left-over ozone. (b) For visible light dissociation (circles are for 520 and squares are for 630 nm light), the calculated α is 1.0151. The error of data point is comparable to the size of the symbol.*

Results of dissociation of ozone in the presence of nitrogen (set 2) are shown in Table 3.2. Up to about 20 torr of nitrogen partial pressure, the slope ($\Delta\delta^{17}O/\Delta\delta^{18}O$) of the left-over O_3 has the same value (0.63) as obtained in set 1 (no nitrogen) experiment. However, the slope increases with the increase in nitrogen partial pressure after 20 torr

and attains a constant value (1.0) beyond 40 torr. The sharp transition of the slope from 0.63 to 1.0 corresponding to nitrogen pressure change (from 20 to 40 torr) is shown in figure 3.3.

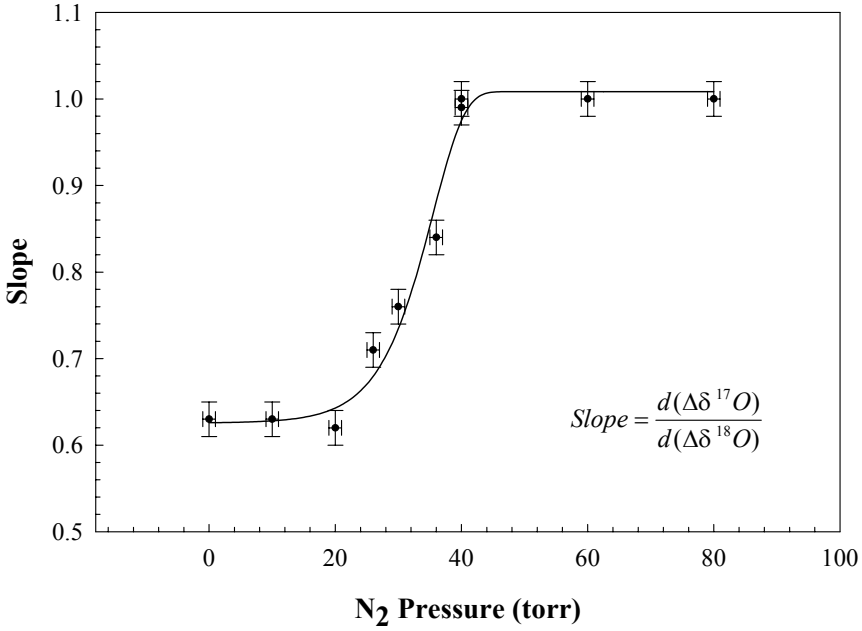

Figure 3.3. *Change in slope connecting $\delta^{17}O$ and $\delta^{18}O$ of the left-over ozone from 0.63 to 1.0 with increasing nitrogen pressure in the reaction chamber during UV photolysis of ozone (of ~ 2 torr). Up to 20 torr of nitrogen pressure the slope is almost constant at 0.63. Subsequently, a rapid increase in slope from 0.63 to 1.0 is observed with the increase of nitrogen pressure from 20 to 40 torr. Beyond 40 torr of nitrogen pressure, the slope remains constant at unity. The errors of the individual slope values are estimated by propagating the errors.*

3.2.4 Discussion

3.2.4.1 Photo-induced kinetic isotope effect

There are several ways in which isotopic substitution can influence the process of molecular photo-dissociation. It can lead to a shift in the absorption spectra (variation of absorption cross-section with wavelength) of a molecule. Isotopic substitution can also remove the symmetry restriction on the molecular wave function, allowing for the occurrence of transitions, which is forbidden for the unsubstituted molecule. It is also noted that isotopic substitution can affect the line intensities in the absorption spectra. Kaye (1991) has presented a review on this subject with illustrations. Miller and Yung (2000) put forward a simple model to explain the photo-induced isotopic fractionation effect and provide a recipe to calculate fractionation resulting from photo-dissociation of

molecules possessing continuous UV absorption spectra and unit photo-dissociation probability. This model is based on the premise that due to shift in the zero point energy between different isotopic species of a molecule, the absorption spectra of the heavy isotopomers are relatively blue shifted and this shift in absorption spectra results in isotopic fractionation in a given wavelength range. The generated isotopic fractionation by this process is not unidirectional. The fractionation is negative (for the left-over ozone) before the peak of the absorption spectra (lower λ side) and positive after the peak (higher λ side) as shown by Miller and Yung (2000) for the D/H ratio variation in the case of water molecule.

Following the Miller-Yung model, we selected the wavelengths 520 ± 2 and 630 ± 4 nm which are on two sides of the peak (600 nm) of the absorption cross-section in the Chappuis band of ozone and carried out ozone photo-dissociation was to detect possible fractionation difference. The isotopic fractionations can be calculated based on zero point energy difference between $^{48}O_3$ and $^{50}O_3$ using the vibrational frequencies of the O_3 isotopomers (Hathorn and Marcus, 2001) and the absorption cross-section of these two isotopomers at a particular wavelength. The zero point energy difference between the symmetric species ($^{16}O^{18}O^{16}O$) and ($^{16}O^{16}O^{16}O$) is 36.2 cm^{-1} and between the asymmetric species ($^{16}O^{16}O^{18}O$) and ($^{16}O^{16}O^{16}O$) is 22.0 cm^{-1}. This leads to fractionations of –18.05 and –10.45 ‰ respectively in the symmetric and asymmetric species of $^{50}O_3$ at 520 nm (using Miller-Yung formula and the absorption cross-section data (DeMore et al., 1997) around 520 nm). Considering the statistical abundances of symmetric and asymmetric species, the total expected fractionation in $^{18}O/\ ^{16}O$ ratio at 520 nm is –13.0 ‰. A similar calculation yields fractionation of 23.18 and 14.9 ‰ respectively in the symmetric and asymmetric species of $^{50}O_3$ at 630 nm, which leads to a total expected fractionation of 17.7 ‰ in $^{18}O/\ ^{16}O$ at 630 nm (see Appendix). However, these amounts of fractionation were not observed. In both cases the product oxygen was depleted and the left-over ozone was enriched (Table 3.3) with respect to the initial ozone with an instantaneous fractionation of about 15 ‰ (Figure 3.2b). Similar enrichment was observed for photo-dissociation with a white lamp, which covers the entire Chappuis band. For the UV photolysis with Hg resonance lamp which emits 184.9 and 253.7 nm photons, the 253.7 nm photons are mainly responsible for the photo-dissociation of ozone since the 184.9 nm line is about 15 times weaker and the absorption cross-section is about 10 times less. The

Miller-Yung model predicts negligible depletion of 0.06 ‰ (see Appendix) in the left-over ozone due to photo-dissociation at 253.7 nm since this wavelength lies near the peak of the absorption band.

3.2.4.2 Photo-dissociation in the Hartley band

In the Hartley band (<300 nm) the 2^1A_1 / $^1B_2 \leftarrow X^1A_1$ transition takes place. Subsequently, a curve crossing between these two upper states and a repulsive state (Valentini et al., 1987; Batista and Miller, 1998) leads to the following two channels of dissociation (Matsumi et al., 2002):

$$O_3 + h\nu \rightarrow O(^1D) + O_2\ (a^1\Delta_g) \quad (3.2)$$

$$O_3 + h\nu \rightarrow O(^3P) + O_2\ (X^3\Sigma_g^-) \quad (3.3)$$

Both these channels are spin-allowed and have quantum yield of 0.9 and 0.1 respectively (Alder-Golden et al., 1982). Two important reactions follow the channel (3.2):

$$O(^1D) + O_3 \rightarrow 2O_2 \quad (3.4)$$

$$O(^1D) + O_3 \rightarrow 2\ O(^3P) + O_2 \quad (3.5)$$

with nearly equal rate coefficients of ~ 1.1×10^{-10} at 298 K (DeMore et al., 1997). The generated $O(^3P)$ from 3.3 or 3.5 can react with O_3 to produce O_2, but the rate coefficient of this reaction is too low (~8×10^{-15}) compared to the rate coefficients of 3.4 and 3.5 (DeMore et al., 1997).

3.2.4.3 Photo-dissociation in the Chappuis band

For the Chappuis band, the *ab initio* calculations show that five electronic states are expected to be involved in that energy range (Arnold et al., 1994). Two of which are singlets ($1\ ^1A_2$ and $1\ ^1B_1$) and three are triplets ($1\ ^3A_2$, $1\ ^3B_1$ and $1\ ^3B_2$). The visible spectra irregularities and diffuse vibrational structures in this band indicate severe predissociation in the transition (Anderson et al., 1991; Anderson and Mauersberger, 1995; Woywod et al., 1997). The absorption spectra in the Chappuis band is due to symmetry allowed $^1B_1 \leftarrow X^1A_1$ transition and the vibronically allowed $^1A_2 \leftarrow X^1A_1$ transition via the ν_3 asymmetric stretch from the ground state (Arnold et al., 1994; Levene et al., 1987; Harold and Valentini, 1987). A conical interaction, which couples the bonded $^1B_1$ state to the dissociative $^1A_2$ state, is responsible for the diffusive nature of the

absorption band (Braunstein and Pack, 1992; Waywod et al., 1997). The dissociation pathway is,

$$O_3 + h\nu \rightarrow O(^3P) + O_2\ (X^1\Sigma_g^+) \qquad (3.6)$$

The basic assumption of Miller-Yung model is the existence of a continuous absorption spectra of the molecule in the wavelength range of interest. This criterion is not strictly valid for the Chappuis band since it has a fine structure. A theory of isotopic fractionation in photo-dissociation involving band structure is still not available but is expected to be quite complex due to combination of vibrational frequency differences among isotopomers, the zero point energy effect and Franck-Condon factor differences. The net result due to various integrating effects will be to reduce the simple Miller-Yung prediction based on zero point energy alone. This probably explains the discrepancy between the observed isotopic fractionation in photo-dissociation at the wavelengths 520 and 630 nm (on the two sides of the Chappuis band absorption peak ~ 600 nm) and the same calculated from the Miller-Yung model.

3.2.4.4 Mass independent isotopic fractionation during photo-dissociation in Hartley band

The covariation plot between $\Delta\delta^{18}O$ and $\Delta\delta^{17}O$ for product oxygen and left-over ozone for the photolysis of ozone in the Chappuis band (Figure 3.1b) reveals that the underlying process is strictly mass-dependent with a slope of 0.54. But the same plot for Hartley band photolysis (Figure 3.1a) yields a slope 0.63 having significant mass independent character. Considering the reactions 3.2 to 3.6, it appears that the crucial difference in ozone photolysis in the Hartley band and the Chappuis band is the presence of $O(^1D)$ in the former case. Wen and Thiemens (1991) have also inferred about the possible role of the excited species $O(^1D)$ and $O_2(^1\Delta)$ in mass independent isotopic fractionation observed in UV dissociation.

Knowing that the $O(^1D)$ yield from ozone photolysis drastically goes down below 300 nm (Matsumi et al., 2002), we have performed ozone dissociation experiment (as a separate set) with different types of lamps (Cd, Hg, Kr) with a set of BK-7 filters (which essentially cuts down the wavelengths below 300 nm). The experimental configurations along with the observed slopes in the left-over ozone are given in Table 3.4. As the Cd lamp has strong lines mostly above 300 nm, the resultant slope is about 0.55 (using a

filter the slope reduces to 0.51). Kr lamp dissociation shows a significant change: 0.55 slope with filter and 0.60 slope without filter. For Hg lamp, the use of filter changes the slope slightly from 0.63 (as mentioned previously) to 0.59.

The results of this set of experiments are quite important since they show that the change in slope in the left-over ozone during ozone photolysis by a particular lamp can be effected only by changing the experimental configuration (by allowing or restricting the wavelengths below 300 nm to enter the chamber).

Table 3.4. *Experimental configuration and results (slope in left-over ozone) for ozone photolysis performed for three different lamps and a set of BK-7 filters to cut-off the wavelengths below 300 nm.*

Lamp	Available wavelengths (nm)[#]	Configuration	Atomic species present	Extent of dissociation (%)	Slope[*]
Cd	228.8 (1500), 298.0	Without filter	$O(^1D)$, $O(^3P)$	13.9	0.55
	(1000), 346.6 (1000),	Without filter	$O(^1D)$, $O(^3P)$	70.6	0.54
	346.7 (800), 361.0	Without filter	$O(^1D)$, $O(^3P)$	83.0	0.54
	(1000), 508.6 (1000),	Without filter	$O(^1D)$, $O(^3P)$	86.2	0.53
	643.8 (2000)	One BK-7 filter	$O(^3P)$	44.0	0.51
Hg	184.9(1000), 253.6(15000), 296.7 (1200), 365.0(2800), 404.7 (1800), 435.8 (4000), 546.1 (1100), 614.9 (1000)	One BK-7 filter	$O(^3P)$	35.6	0.59
		Three BK-7 filters	$O(^3P)$	5.7	0.59
Kr	116.5 (200), 123.6	Without filter	$O(^1D)$, $O(^3P)$	68.0	0.60
	(650), 427.4 (1000),	Without filter	$O(^1D)$, $O(^3P)$	82.0	0.60
	431.9 (1000), 437.6	One BK-7 filter	$O(^3P)$	7.4	0.55
	(800), 446.4 (800),	One BK-7 filter	$O(^3P)$	11.4	0.55
	557.0 (2000), 587.0 (3000)				

Considering the totality of the reactions 3.2 to 3.5 and the results of the experiments described above, two dissociation channels needs to be discussed to decipher the source for the mass independent fractionation in case of Hartley band dissociation: (i)

[#] The figures inside the bracket denote the relative strengths of the lines.

* After propagation of errors, the uncertainty in individual slope value is less than 10 %.

Direct UV dissociation step (reaction 3.2), and (ii) $O(^1D)$ assisted O_3 dissociation steps (reactions 3.4 and 3.5).

3.2.4.5 Source of mass independent isotopic fractionation in Hartley band photo-dissociation

Set 2 experiments were designed to address the question of mass independent fractionation since the presence of nitrogen with O_3 in the reaction chamber during UV photolysis provides a pathway for removal of $O(^1D)$. Nitrogen is an effective quencher of $O(^1D)$ with a rate constant ~ 2.6×10^{-11} cm^3/molecule-sec (DeMore et al., 1997), which is five times less than that of the $O(^1D) + O_3$ reaction. Figure 3.3 shows the effect of nitrogen on the resultant slope during UV photolysis. There is a sharp change in the slope with increase in the nitrogen pressure, which can be interpreted in terms of $O(^1D)$ removal. The effective quenching of $O(^1D)$ is more with increase in concentration of nitrogen in the chamber, making the contribution of $O(^1D)$ in net O_3 dissociation via reactions 3.4 and 3.5 less. This is evident from the gradual transition of the value of slope from 0.63 to 1.0 with increase in the nitrogen pressure from 20 to 40 torr. The slope attains a constant value of 1.0 for nitrogen pressure higher than 40 torr indicating a saturation effect in the quenching of $O(^1D)$ by nitrogen. This leads to the conclusion that O_3 dissociation at relatively high nitrogen pressure is only through R1, the direct dissociation pathway. This step then ought to represent a process characterized by pure mass independent fractionation with a slope of unity. This is the first experimental demonstration that pure UV dissociation of ozone bears a mass independent slope intriguingly similar to that obtained in its formation process. The observed slope of 0.63 without nitrogen quencher, therefore, has to result from a combination of the two dissociation pathways – the pure photo-dissociation and pure $O(^1D)$ mediated dissociation.

The instantaneous fractionation factor for pure photo-dissociation calculated following Eqn. 3.1 (using 4 data points for nitrogen pressure from 40 to 80 torr having slope value of 1.0) gives a value 1.0071, which, as expected, is less than that of the no-nitrogen case (set 1: α = 1.0176) combining the two channels of dissociation. The dissociation without nitrogen quencher can be thought of as a combination of the two processes each working independent of the other such that $\alpha_{total} = \alpha_{photo} + \alpha_{O(^1D)}$.

Therefore, the effective fractionation factor for the $O(^1D)$ mediated dissociation is 1.0104. It is of interest to enquire about the underlying process responsible for 10.4 ‰ fractionation in the $O(^1D)$ reaction with O_3. Since lighter molecules collide more frequently due to their higher velocity and the collision rate ratio is proportional to the square root of the reduced mass ratio, one can estimate the isotopic fractionation arising out of this effect. This turns out to be about 5 ‰ considering collision between ^{16}O with $^{48}O_3$ and ^{16}O with $^{50}O_3$. The remaining 5 ‰ seems to be contributed by the effect of zero point energy difference on the reaction rates. The dissociation of ozone by $O(^1D)$ is typical example of an 'abstraction reaction' and involves break-down of one O–O bond in the ozone molecule and formation of a new O – O bond between the incident $O(^1D)$ and the ejected atom. As in any abstraction reaction (Shiner, 1975), it is slightly easier to break bonds involving lighter isotopes compared to those involving heavier isotopes. As a result, the reaction rate is slightly higher for the lighter isotopomer. An exact calculation of this effect in the present case is difficult because stretching motions of the transition state is involved (Shiner, 1975). However, an idea of the magnitude of fractionation can be obtained by using the high temperature limit of the Bigeleisen-Wolfsberg formula for the kinetic isotope effect under the Harmonic Oscillator approximation as summarized by Van Hook (1970). The isotope effect is given by $(\mu_2/\mu_1)^{0.5}$, where μ refers to the reduced mass of the two approaching particles (^{16}O atom and ozone molecule) and the subscripts 2 and 1 refer to the heavy and light isotopomers of ozone (Van Hook, 1970). This produces again 5 ‰ fractionation which is consistent with the required amount. The high temperature limit is justified because the colliding $O(^1D)$ imparts its large electronic energy of 1.97 eV to the transition state molecule during the collision.

3.2.4.6 Non-RRKM effect during O_3^* dissociation

To explore the reason behind the fractionations mentioned above, it would be important to consider why UV dissociation gives a mass independent slope, but the dissociation in the visible range does not. The first step of photo-dissociation dynamics of a molecule is the formation of electronically and vibrationally excited molecule. Interestingly, a similar excited intermediate also results during ozone formation by collision of O-atom with O_2-molecule. The excited molecule in both the cases can dissociate through different channels. As discussed in Chapter I, the mass independent

isotopic fractionation during ozone formation has been explained by a novel approach by introducing a small departure from the complete statistical randomness of the standard RRKM method (Hathorn and Marcus, 1999, 2000; Gao and Marcus, 2001) (see Chapter I, § 1.3.3 for a brief discussion). The first step in this scenario is the formation of a short-lived O_3^* complex by O – O_2 collision. Subsequent redistribution of the total energy among the vibrational-rotational modes of this vibrationally excited transient molecule proceeds at some finite rate and may be incomplete during the typical life-time of this excited molecule (the non-RRKM effect). This non-statistical effect reduces the effective density of the available quantum states and consequently, the unimolecular dissociation rate ($k_{EJ} = N_{EJ}^{+} / h\rho_{EJ}$) increases. The reduction of the density of quantum states is more for the symmetric molecules than for the asymmetric molecules (since there are fewer dynamical coupling terms in the symmetric than in the asymmetric molecules).

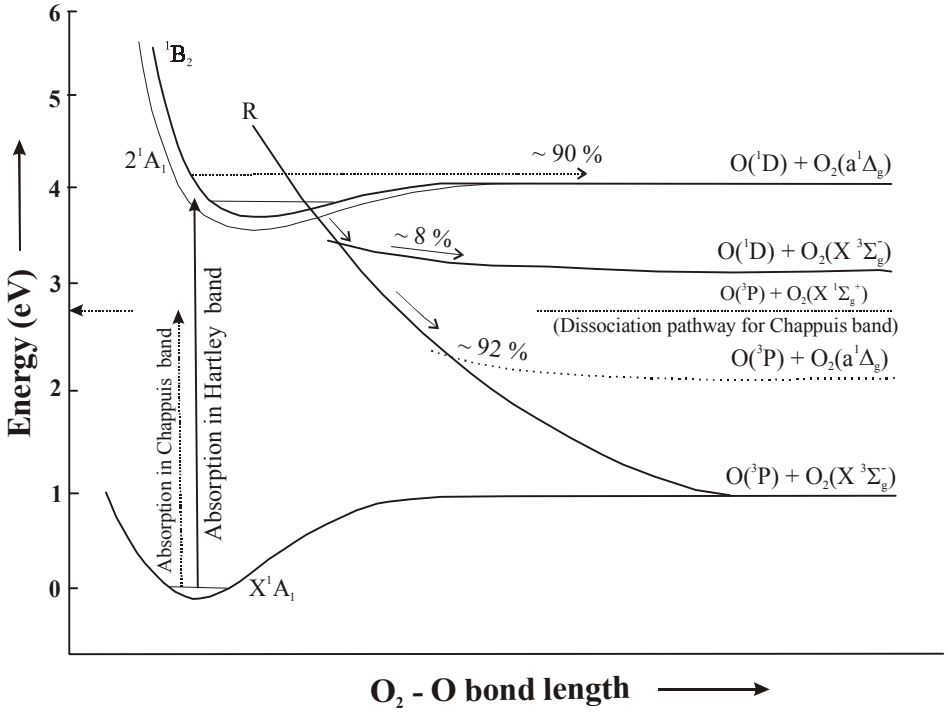

Figure 3.4. *Schematic diagram of the potential energy curves as a function of dissociation coordinate with the possible dissociation channels for the Hartley and the Chappuis band. Dissociation in Hartley band yields $O(^1D)$, whereas the Chappuis band dissociation produces ground state oxygen atom (O^3P).*

It was shown by detailed calculations that this small non-statistical effect amplifies as a large mass independent isotopic effect in stabilized ozone molecules. A similar situation may be applicable for the photo-dissociation of ozone because of the formation of the intermediate excited state (O_3^*) by absorbing photons (UV or visible). Absorption of photons in the Hartley band will lead to the formation of excited O_3^* species in the $^1B_2$ (or 2^1A_1) electronic state (shown in Figure 3.4) similar to the formation of excited state during ozone formation in the X^1A_1 state (Hathorn and Marcus, 1999). A non-statistical energy distribution can take place within various modes of O_3^*, which may be incomplete within its typical life-time ultimately leading to a mass independent isotopic effect. However, for the Chappuis band, pre-dissociation (Anderson et al., 1991, 1995; Woywod et al., 1997) plays a dominant role. This implies a larger life-time during which the molecule gets enough time for randomization of energy. Therefore, a non-statistical symmetry dependent effect would not take place.

3.2.5 Conclusion of Photo-dissociation Study

In photon interaction with ozone isotopically lighter isotopomers are preferentially dissociated resulting in the formation of lighter oxygen and enriched left-over ozone. However, photo-dissociation in the Hartley band (by UV light) and Chappuis band (by visible light) are characteristically different – the former produces oxygen which is mass-independently fractionated while the latter produces oxygen, which is lighter in strictly mass-dependent fashion.

The recent Gao-Marcus theory explains the mass-independent enrichment in ozone formation by involving incomplete randomization of energy among the various modes of the ozone complex (a non-RRKM effect) formed by collision of O-atom and O_2-molecule. A similar situation seems to be operative in case of photo-dissociation but the energy is provided by photon absorption. Therefore, the same Gao-Marcus theory can explain the mass-independent dissociation in UV photolysis of ozone. However, for the Chappuis band, pre-dissociation is mainly responsible for the ozone destruction and this involves large life-time of the complex thereby minimizing the non-RRKM effect and resulting in a mass-dependent fractionation.

3.3 PART B: SURFACE INDUCED DISSOCIATION OF OZONE

3.3.1 Motivation

The present set of experiments was planned for the isotopic characterization of the dissociation process when ozone molecules strike a surface. In many laboratory experiments surface dissociation of ozone can be important. For example, it was observed that the anomalous isotopic enrichment in the oxygen formed by ozone photo-dissociation is substantially less than that for ozone formation from oxygen (Bhattacharya and Thiemens, 1988; Wen and Thiemens, 1990, 1991), though the source of the anomalous fractionation for both the cases can be traced to the formation of an activated complex involving vibrationally excited ozone molecule. The smaller enrichment in the dissociation process is presumably due to the interference by surface effects operating in the low-pressure dissociation experiments. Again, to explain the increase in enrichment with temperature during thermal dissociation it was proposed that increased collision rate at higher temperature results in more effective gas phase reaction. This implies a reduced role of surface interaction of ozone molecules and higher net enrichment at higher temperature. The need to test these propositions provided the motivation for our present study.

Another goal is to understand the mechanism of dissociative reactions on surface followed by chemi-adsorption, which are still modeled by empirical concepts without adequate microscopic picture of the underlying processes (Gregg, 1961). Isotopic fingerprints of the products can sometimes provide valuable insight. For example, Winter (1958) showed that oxygen adsorbed on metal oxide surfaces undergoes exchange with lattice oxygen through isotopic methods. Since ozone is highly reactive, its dissociation on glass surface provides an easy set up for such studies.

In the present experiment, dissociation of ozone on two different surfaces, pyrex and quartz was carried out and the isotopic fractionation between the left-over ozone and product oxygen was studied.

3.3.2 Experimental Procedure

Ozone was produced by UV photolysis of ultra-pure oxygen (99.99% purity) at pressure of 180 torr. The same 5-liter spherical Pyrex vessel described in §2.2.1 was used as the reaction chamber. A resonance Krypton lamp (116.5 and 123.6 nm) operated inside

an Evenson cavity excited by a 120 watt, 2450 MHz microwave generator was used as the UV source.

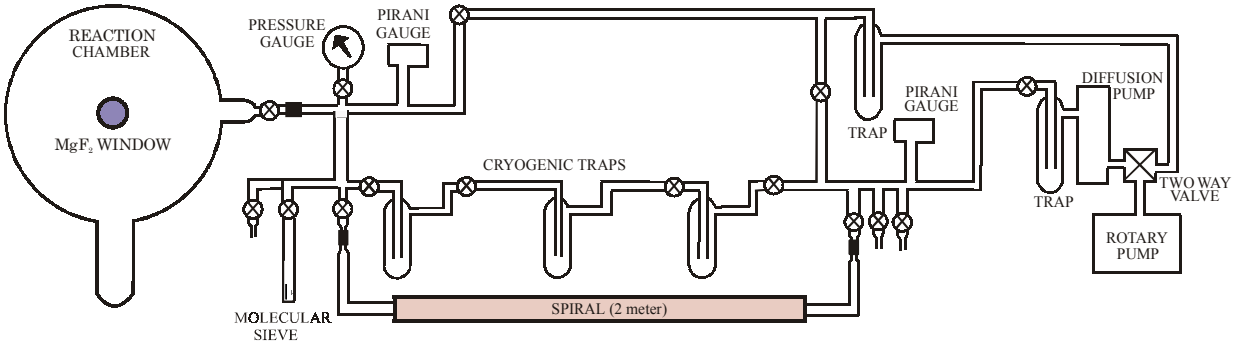

Figure 3.5. *Schematic diagram of the vacuum manifold used for surface dissociation study. The reaction chamber has a cold finger at the bottom and is fitted with a MgF_2 window. Ozone was made to pass through the spiral for effecting surface dissociation.*

The photolysis time for all the experiments were kept constant at 180 minutes. The produced ozone was separated by first condensing it at the bottom trap with LN_2 and pumping the remaining oxygen till a few mtorr pressure (vapor pressure of liquid ozone) was obtained. For effecting dissociation at the inner surface of glass, the following steps were followed. LN_2 was removed and ozone was transferred to a chamber (volume ~10 cc) cooled by LN_2. The unfrozen residual gas amount for all the experiments were about 2 μmole. Two different spirals made of pyrex and quartz (each of them made from 2 meter long and 8 mm inner diameter tube) were used (Figure 3.5 shows the complete set-up of the experiment). The spiral as well as the manifold was kept opaque with aluminum foil wrapping. The liquid ozone was released by removing LN_2 and made to pass through the spiral by keeping another chamber (volume ~10 cc) cooled by LN_2 at the other end of the spiral. After passing through the spiral, the residual ozone gets collected in this second chamber. Sufficient time was given to get the residual ozone in the second chamber and the unfrozen fraction (supposed to be oxygen, produced from the breakdown of ozone by surface collision) was collected in a sample bottle with molecular sieve at LN_2 temperature. It was estimated that about 15 % of the initial ozone breaks down in the first pass. To get different fractions of product oxygen, ozone was passed through the spiral several times and each time residual ozone was collected first and then the product oxygen. As the number of passes increased the percentage breakdown of ozone decreased

significantly. The residual ozone was finally collected in a sample bottle (volume = 1 cc) with molecular sieve at LN_2 temperature. Ozone was converted to oxygen by repeated freezing and heating of molecular sieve containing ozone.

Oxygen isotopic measurements were done on a triple collector mass spectrometer (model GEO 20-20 of Europa Scientific) with typical error of 0.2 ‰ and 0.1 ‰ for $\delta^{17}O$ and $\delta^{18}O$ respectively. The yield of ozone and product oxygen was estimated following the procedure described in § 3.2.2.

3.3.3 Results

The isotopic composition ($\delta^{17}O$ and $\delta^{18}O$) of the left-over ozone and product oxygen along with their amount are shown in Table 3.5 for the pyrex and quartz spirals. The initial composition of ozone was calculated by mass balance, knowing the amount and composition of the left-over ozone and product oxygen. The amount of ozone initially produced (sum of the amount of left-over ozone measured as oxygen and product oxygen) by photolysis shows large variation (from about 23 to 57 μmole) due to variation in the output of the Kr lamp. However, the $\delta^{18}O$ of the initial ozone varied only by a small amount (mean ~104 ± 2 ‰). $\Delta\delta^{17}O$ and $\Delta\delta^{18}O$ (Table 3.5) denote the enrichment or depletion with respect to the initial ozone composition. The data show that dissociation of ozone yields isotopically light oxygen, while enriching the left-over ozone pool. To increase the extent of fractionation, the ozone was passed through the spiral several times. With the increased amount of dissociation, the amount of left-over ozone decreased and gradually became isotopically heavier. Figure 3.6 shows the covariation plot between $\Delta\delta^{17}O$ and $\Delta\delta^{18}O$. When the fractionation of the ozone reservoir is small (less than ~15 ‰ with respect to the initial composition), the slope of the covariation plot is about one and with the increase of fractionation the slope of the line decreases. Beyond 25 ‰, the points do not fall on the slope one line rather they yield a slope value of about 0.75. The isotopic behavior does not change significantly with the change of the spiral material from pyrex to quartz.

Table 3.5. *Table showing results of the surface induced dissociation experiment. Results for the two different surfaces, made of pyrex glass and the quartz glass are shown separately. The amount of ozone is measured as oxygen after converting O_3 to O_2 (as described in the text). The initial composition of ozone was calculated from the mass balance of the two component (i) leftover ozone and (ii) product oxygen.$\Delta\delta^{17}O$ and $\Delta\delta^{18}O$ represent enrichment and depletion for ozone phase and oxygen phase respectively with respect to the initial composition.*

Amount of initial ozone (μmole)	Initial ozone* composition		Amount of left-over ozone (μmole)	Amount of product oxygen (μmole)	Left-over ozone*				Product oxygen*			
	$\delta^{17}O$ (‰)	$\delta^{18}O$ (‰)			$\delta^{17}O$ (‰)	$\delta^{18}O$ (‰)	$\Delta\delta^{17}O$ (‰)	$\Delta\delta^{18}O$ (‰)	$\delta^{17}O$ (‰)	$\delta^{18}O$ (‰)	$\Delta\delta^{17}O$ (‰)	$\Delta\delta^{18}O$ (‰)
Pyrex Glass												
39.3	97.5	100.9	30.0	9.3	101.5	95.8	3.9	5.1	84.8	84.5	-12.7	-16.4
31.5	97.4	103.4	22.6	8.9	102.6	99.0	5.1	6.5	84.4	87.0	-13.1	-16.4
41.8	96.5	103.8	24.5	17.3	104.5	102.0	7.9	9.8	85.3	89.9	-11.2	-13.9
36.5	94.8	105.8	19.1	17.4	107.8	107.0	13.1	14.0	80.4	90.4	-14.4	-15.4
29.5	95.3	103.9	11.7	17.8	105.5	96.3	10.2	11.7	88.6	92.3	-6.7	-11.6
25.8	96.1	105.6	8.0	17.8	106.5	108.4	10.4	20.9	91.4	96.3	-4.7	-9.4
27.8	92.9	106.0	7.8	20.0	111.7	116.5	18.8	26.0	85.6	95.8	-7.3	-10.1
22.9	93.4	106.2	3.0	19.9	119.6	128.0	26.2	40.6	89.5	100.1	-4.0	-6.1
42.0	96.7	104.8	5.0	37.0	119.9	125.9	23.2	39.2	93.6	99.5	-3.1	-5.3
Quartz Glass												
56.8	97.3	105.2	51.0	5.8	100.2	108.7	3.0	2.4	71.4	83.9	-25.9	-21.3
52.2	94.8	104.9	42.7	9.5	99.0	108.8	4.2	3.8	75.9	87.8	-18.9	-17.2
39.7	95.3	106.6	26.7	13.0	106.7	116.3	11.4	9.8	71.8	86.5	-23.5	-20.1
37.3	88.7	100.5	23.8	13.5	94.8	108.9	7.1	8.4	75.3	85.7	-12.5	-14.8

* The errors in measurements of $\delta^{18}O$ and $\delta^{17}O$ (estimated from some repeat measurements) are 0.1 and 0.2 ‰ respectively.

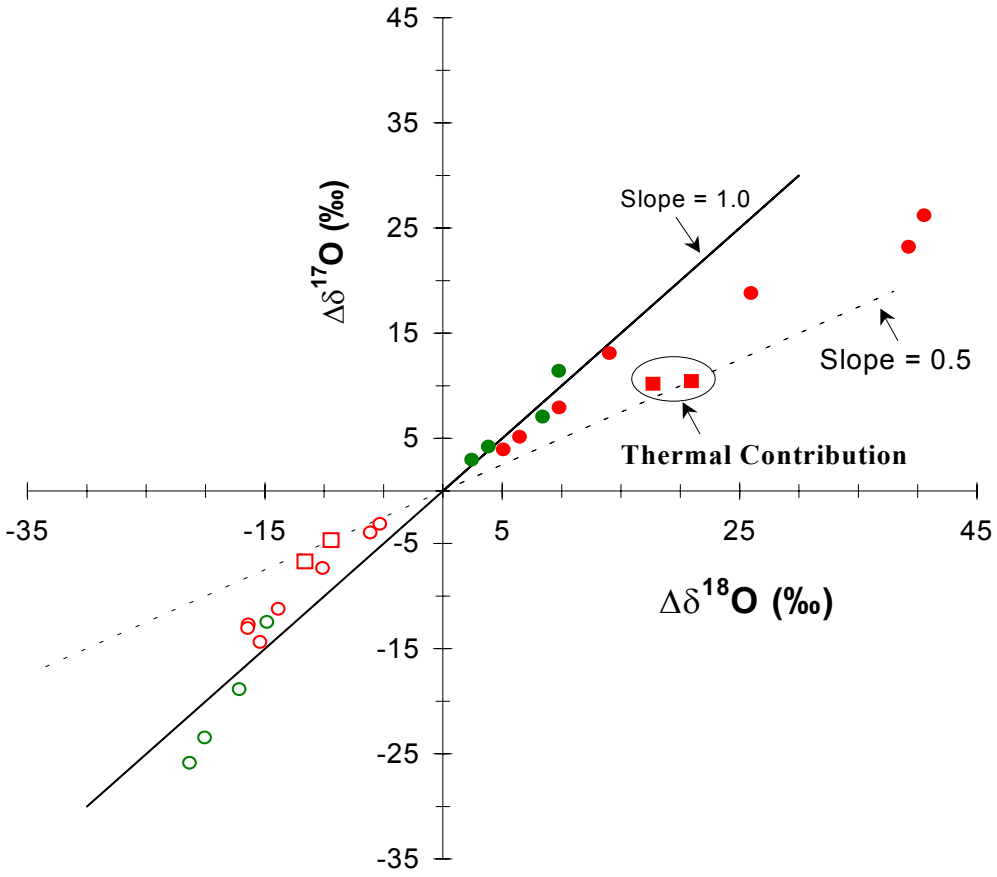

Figure 3.6. *Covariation plot of $\Delta\delta^{18}O$ and $\Delta\delta^{17}O$ for surface induced dissociation process. The initial composition of ozone is calculated by mass balance of the two fractions (left-over ozone and product oxygen). The upper right quadrant represents the left-over ozone component (filled symbols) and the lower left quadrant the product oxygen (unfilled symbols), which is enriched in light isotope. The circles and the triangles represent the results for pyrex and quartz surfaces respectively. For small amount of fractionation, the slope is around unity. As the fractionation increases, the slope decreases. The two points (encircled squares) represent a different experimental condition effecting thermal dissociation as described in the text. The errors of the individual data points are comparable to the size of the symbols.*

In order to determine the fractionation factor α, we assume a Rayleigh fractionation function of the form of Eqn. (3.1). Figure 3.7 shows the correlation diagram between Δ and ln(f). The best fit of all the data points gives the instantaneous fractionation factor for the left-over ozone as $\alpha_{\text{left-over ozone}} = 1.017$ indicating that the product oxygen is depleted by about 17 ‰ relative to the initial ozone composition.

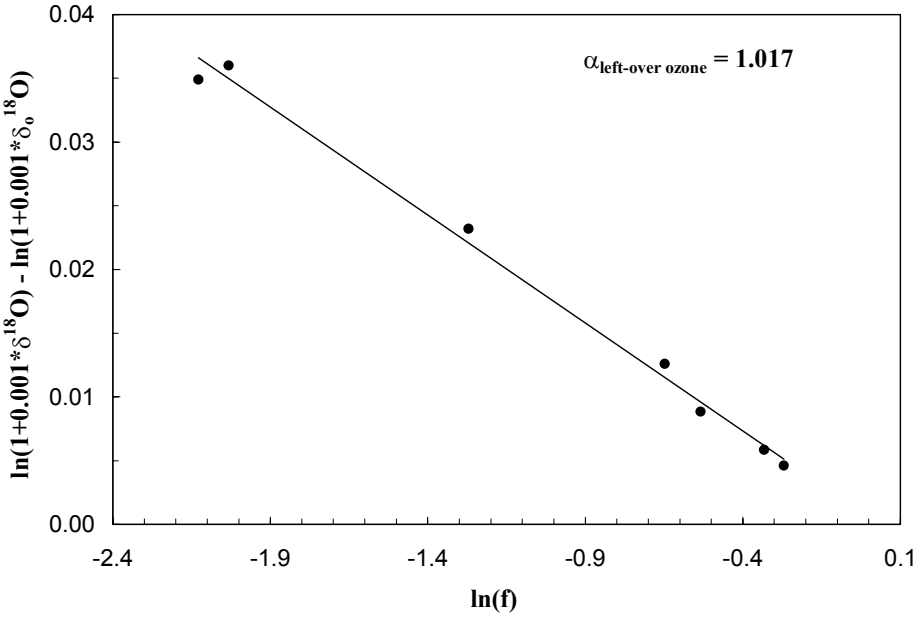

Figure 3.7. *Plot for calculating the fractionation factor for the surface dissociation process using a Rayleigh model. X-axis represents the fraction left in the O_3 pool. Data plotted in the Y-axis are normalized to the initial composition of ozone. As the fraction in the O_3 pool decreases, the delta value increases accordingly giving a fractionation factor (α) of 1.017. The error of each data point is comparable to the size of the symbol.*

3.3.4 Discussion

The dissociation of ozone yields isotopically light oxygen similar to that of the product of photo-dissociated ozone and thermally (< 90ºC) dissociated ozone (Wen and Thiemens, 1990, 1991, Kim and Yang, 1997) but does not follow the conventional mass fractionation pattern (slope value of half). Instead, it gives rise to a slope value of unity in the covariation plot of $\Delta\delta^{17}O$ and $\Delta\delta^{18}O$ (Figure 3.6) surprisingly similar to the slope observed in case of formation of ozone (see initial ozone composition in Table 3.5).

Why the surface dissociation of ozone produces oxygen with mass independent fractionation is a puzzling question but one can invoke a scenario using the concepts of recently proposed Gao-Marcus theory (Gao and Marcus, 2001; see Chapter I, § 1.3.3 for a brief discussion), which explains the mass independence in case of ozone formation. Gao-Marcus theory proposes that during ozone formation by $O + O_2$ recombination reaction a short-lived O_3* complex is formed. Subsequent redistribution of the total energy among the rotational-vibrational modes of this excited transient molecule proceeds at some finite rate and may be incomplete during the typical life-time of this complex (non-RRKM effect). This non-statistical effect reduces the effective density of the available quantum

states and consequently the unimolecular dissociation rate of the complex increases decreasing the probability of formation of a stable ozone molecule. The reduction of the density of states is more for the symmetric molecule (which has more share of lighter isotopes) than for the asymmetric molecules (since there are fewer dynamical coupling terms in the symmetric molecule). It was shown that this small non-statistical effect amplifies as a large mass independent isotope effect in stabilized ozone molecules.

For surface dissociation of ozone, the first step involves chemi-sorption of ozone molecule on the surface as it happens in the case of oxygen, which is slightly less reactive. We postulate that the ozone molecule forms an activated complex (Figure 3.8) with a reactive atom residing on the surface (Cristmann, 1991). This activated complex is a transient species and may dissociate after its typical lifetime in the following way,

$$O_3 + \text{Surface (W)} \rightarrow (O_3W)^* \rightarrow O(^3P) + O_2\,(X^1\Sigma_g^+) + W^* \qquad (3.7)$$

The ozone complex being confined to the surface has less degrees of freedom and can only have restricted rotational and vibrational motions. This reduces the density of states and makes the activated complex short-lived. We then can consider a non-statistical Gao-Marcus model, which favors the asymmetric molecules for its intra-molecular energy redistribution. This reduces the dissociation rate constant of the asymmetric molecules and results in mass independent isotopic enrichment in the left-over ozone. The product oxygen is correspondingly equally depleted in ^{17}O and ^{18}O. This explanation is at present speculative and needs to be tested experimentally and theoretically.

To achieve larger fractionation, the ozone had to go through the spiral many times. For example, to get around 25 ‰ enriched ozone, the required time was nearly 6 hours and some amount of thermal dissociation in this time cannot be avoided. Therefore, higher amount of fractionation (> 25 ‰) arises due to combination of two processes i.e. surface interaction and gas phase dissociation. The room temperature thermal dissociation yields a mass-dependent slope (~ 0.5) in contrast to the surface dissociation (slope ~1.0) and the admixture of these two components produces a resultant slope with value less than one. This explanation is supported by the thermal dissociation data (points encircled in Figure 3.6, representing the situation when the ozone was kept within the spiral for about 8 hours at room temperature). They define a slope of around half, which is expected in case of thermal decomposition at room temperature (Wen and Thiemens, 1990).

Recently Bhattacharya et al. (2002) (also see Chapter II) studied the pressure dependency of isotopic enrichment in ozone (produced from oxygen photolysis at different oxygen pressures ranging from 8 to 700 torr). They explained the observed enrichment pattern for pressure upto 15 torr by considering simultaneous formation and dissociation in gas phase. However, the enrichment pattern observed below 15 torr (equal enrichment in ^{17}O and ^{18}O with lower magnitude compared to that observed at 15 torr) did not fit with the proposed hypothesis. In that pressure range, the ozone production was less than 0.05 μmole/min (Bhattacharya et al., 2002; Chapter II, § 2.3) and ozone decomposition by interaction with the surface was assumed to be significant. The results obtained in the present experiment provide support for this assumption.

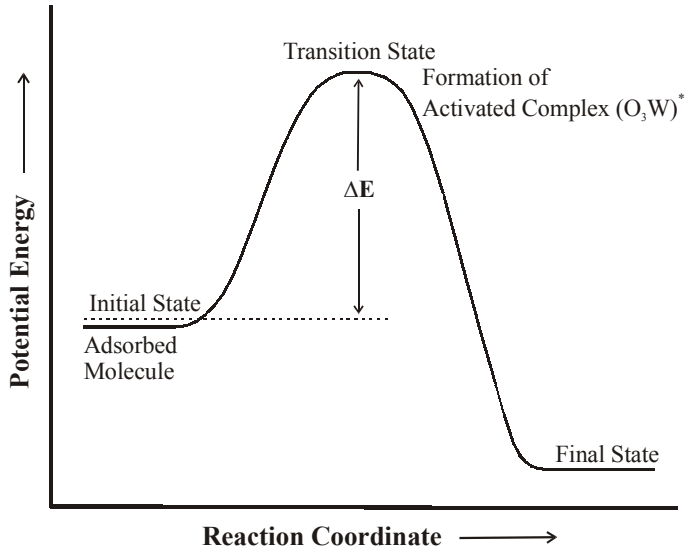

Figure 3.8. *Formation of an activated complex $(O_3W)^*$ by adsorption of ozone molecule on a surface (ΔE represents the heat of adsorption). The energy redistribution among all its rotational/ vibrational states may be incomplete during its typical lifetime resulting in a mass independent isotopic effect in the products.*

3.3.5 Conclusion of Surface Induced Dissociation Study

The isotopic behavior of ozone during dissociation on glass surface is anomalous. The process leads to faster dissociation of lighter isotopomers and surprisingly, the rate constant is equally less for ^{17}O and ^{18}O containing molecules. No noticeable variation was observed with the change in the surface material. As the experimental time increases, the

mass independent effect is reduced due to the admixture of products from thermally dissociated ozone.

It is postulated that the dissociation of ozone on a surface takes place by dissociative adsorption. In this mechanism, an activated complex $(O_3W)^*$ formed as an intermediate. The mass independent isotopic fractionation arises due to non-statistical (non-RRKM) energy randomization within the activated complex resulting in lesser dissociation rate of the asymmetric intermediates compared to the symmetric one.